First-principles calculations of domain wall energies of prototypical ferroelectric perovskites

Xueyou Zhang ^{a,b, &}, Bo Wang ^{b,&}, Yanzhou Ji ^b, Fei Xue ^b, Yi Wang ^{b,*}, Long-Qing Chen ^b, Ce-Wen Nan ^a

&Equal contribution: X.Y. Zhang and B. Wang *Corresponding author: yuw3@psu.edu (Y. Wang)

Abstract

Ferroelectric domain walls play a critical role in determining the polarization switching kinetics and physical properties in ferroelectric materials. There have been extensive studies on identifying the domain wall structures and domain wall energies. Nevertheless, the predicted domain wall energies tend to vary a lot for the same type of domain walls, and it remains elusive under what conditions the non-Ising type domain wall is more stable than the Ising type. In this work, we performed first-principles calculations to evaluate the structures and energetics of several types of domain walls for two prototypical tetragonal ferroelectric perovskites, PbTiO₃ and BaTiO₃, including charge-neutral 90° domain walls, Ising-type and Ising-Bloch-type 180° domain walls with various orientations. We adopted three schemes of structural optimization to optimize the domain wall structures and extract the domain wall energies by carefully eliminating the contribution from strain energies. We discussed how the choice of the schemes influence the calculation results and their applicable conditions. We found that the anisotropy of domain wall energy for Ising-type 180° walls is larger in BaTiO₃ than that in PbTiO₃. The emergence of Bloch component in PbTiO₃ can lower the domain wall energy and reduce its anisotropy. This work offers a more accurate method for predicting the domain wall structures and energetics of ferroelectrics. The calculation results can be useful for understanding of stability of ferroelectric domain walls with high-index orientations and non-Ising characteristics, which is of critical importance in developing domain wall nanoelectronics.

Key words: ferroelectric domain walls; BaTiO₃; PbTiO₃; perovskite oxides; first-principles calculations

1. Introduction

Ferroelectric materials are featured by the presence of spontaneous polarization that can be reversed by an applied electric field. One of the salient microstructural characteristics of ferroelectric materials is the formation of polar domains that are separated by domain walls (DWs). The DWs have been demonstrated to exhibit behaviors different from the domains,

^a School of Materials Science and Engineering, State Key Lab of New Ceramics and Fine Processing, Tsinghua University, Beijing, 100084, China

^b Department of Materials Science and Engineering, The Pennsylvania State University, University Park, PA, 16802, United States

such as reduced mechanical compliance[1], enhanced dielectric permittivity[2, 3], increased electronic conduction[4, 5], and improved photovoltaic effects[6, 7]. Moreover, the dynamics of DWs during ferroelectric switching is closely related to the fatigue and degradation behaviors of ferroelectric materials[8]. Therefore, understanding the statics and dynamics of DWs is of great importance not only for harnessing their distinct properties but also for enhancing the reliability of ferroelectrics-based electronic devices.

There have been extensive theoretical efforts devoting to understanding the structure and kinetics of DWs, including the Landau-Ginzburg-Devonshire (LGD) theory and first-principles calculations. The LGD theory has been utilized to derive closed-form solutions of the polarization distribution, thickness, and formation energy of ferroelectric DWs[9, 10]. The parameters used in the LGD model can be evaluated by fitting to experimental measurements of the bulk materials[10]. On the other hand, first-principles calculations can predict the structures and energies of DWs free of fitting parameters and provide insights on the configuration and properties of DWs from the atomistic and electronic perspectives.

However, the DW energies obtained from the first-principles calculations may be influenced by the structural optimization schemes [11, 12]. In general, there are three types of schemes to relax the DW supercell in literature: (i) both the lattice vectors and the atomic positions are fully relaxed, as adopted in Ref.[13-15]; (ii) only the lattice vector normal to the DW plane and the atomic positions are relaxed, while the other two lattice vectors parallel to the DW plane are fixed, as adopted in Ref.[12, 16]; (iii) only the atomic positions are relaxed while keeping the three lattice vectors fixed, as adopted in Ref.[4, 11, 15, 17, 18]. In addition, symmetry constraints may be imposed to the atomic relaxation, such as the mirror operation and inversion centers. One of the main objectives of this work is to compare and discuss the applicability of those schemes under different constraints.

DWs of perovskite oxides such as PbTiO₃ (PTO) and BaTiO₃ (BTO) have been extensively investigated using first-principles calculations. Most previous studies focused on 90° DWs and (100)- or (110)-oriented 180° DWs[11, 16, 18-20]. The investigation on 180° DWs parallel to a high-index plane is limited. Li et al.[12] investigated (410)-oriented as well as (100)-oriented 180° DWs of tetragonal BaTiO₃ and found no preferred orientation based on the close DW energies of (100)- and (410)-oriented DWs. Based on the LGD theory, the anisotropy of polarization vectors at the DW in tetragonal BaTiO₃ was investigated[21, 22]. However, the general anisotropy of 180° DW energies in tetragonal ferroelectric perovskites has not been investigated. The DW anisotropy is of significant importance for understanding the orientation preference of DW formation and motion in ferroelectric crystals.

The chirality of ferroelectric DWs enables another degree of freedom to be tuned for logic and memory device applications[23]. However, there remains large discrepancy in the existing literature for the presence and stability of chiral DWs. For example, the 180° DWs of perovskite oxides have long been considered as pure Ising-type DWs, across which the polarization vectors simply change the magnitude while reversing their directions. Lee et al.[16, 24] and Behera et al.[15] have found Bloch- and (or) Néel-component in 180° DWs in PbTiO₃ and LiNbO₃ in addition to the predominant Ising-component using first-principles calculations. Phenomenological analysis and phase-field simulations have found that the emergence of non-Ising components may be ascribed to the flexoelectric effect[21, 22]. Using first-principles calculations, Wang et al.[17] studied atomic and electronic structure of 180°

DWs in PbTiO₃ and found that the Bloch-type component originates from the large displacement of Pb and Pb-O hybridization at the DWs. The existing studies of Bloch-type component are mainly focused on DWs with low crystallographic indices in the tetragonal phase with only a few exceptions[12, 21]. Nevertheless, it remains unknown whether there are non-Ising or chiral components in DWs with high crystallographic indices.

In this work, we systematically investigate the DW energies of two prototypical tetragonal ferroelectric perovskites: PbTiO₃ and BaTiO₃. We adopt three structural optimization schemes to calculate the structures and energetics of the DWs and compare their conditions of applicability which are described in Section 2. We also evaluated and discussed the anisotropy of the 180° DW energies in BaTiO₃ and PbTiO₃ in Section 3, which suggests that BaTiO₃ exhibits a larger anisotropy than PbTiO₃ in terms of the 180° DW energy. It is found that the non-Ising type component is observed in all 180° DWs of PbTiO₃ and is energetically more favorable than its Ising-type counterpart, regardless of orientations. We summarized our findings in Section 4.

2. Theoretical Details

2.1 Method of calculation

We perform first-principles calculations based on density functional theory using Vienna Ab initio Simulation Package (VASP). We employ the projector-augmented wave (PAW) method[25-27] with the local-density approximation (LDA)[28] and an cutoff energy 520 eV. The projector augmented wave potentials include 6 valence electrons for O (2s²2p⁴), 12 for Ti (3s²3p⁶3d²4s²), 14 for Pb (5d¹⁰6s²6p²), and 10 for Ba (5s²5p⁶6s²). The geometry optimizations are performed using the conjugate gradient algorithm until forces acting on the ions are less than 10⁻³ eV/Å. The change of total energy was converged to 10⁻⁶ eV. Γ-centered **k**-point meshes for every supercell in this work are summarized in Table 1. Crystal and DW structures are plotted using VESTA[29].

2.2 Domain wall structures

The present work focuses on two prototypical ferroelectric perovskite oxides, PbTiO₃ and BaTiO₃. PbTiO₃ undergoes a phase transition from a paraelectric cubic phase to a ferroelectric tetragonal phase at 763 K and remains the tetragonal phase down to 0 K. BaTiO₃ undergoes a series of structural phase transitions from a cubic to a tetragonal phase at 393 K, then to an orthorhombic phase at 278 K, and finally to a rhombohedral phase at 183 K. In this work, we only consider the tetragonal phase of both materials. DWs in tetragonal ferroelectric phase can been classified into 180° and 90° types[11, 16, 18-20], where the polarization directions on the two sides of the DW are antiparallel and perpendicular, respectively. Table 1 summarizes the information of all supercells for DW calculations in this paper.

 inversion centers, as shown in Fig. 1(a)-(b). Furthermore, we construct the mixed Ising-Bloch-type (IB) DWs with anti-parallel Bloch-type component by displacing the A atoms in two DWs at the center and the boundary of the supercells along +y and -y direction, respectively. The two DWs at the center and the boundary of the supercells are equivalent. Note that we only present the results of IB-type DWs for tetragonal PbTiO₃ here because our calculations show that the relaxation of a preset IB-type DW for tetragonal BaTiO₃ lead to unstable supercell structures.

We also construct supercells containing Ising-type 180° DWs with orientations different from (100), which we termed as high-index domain wall planes. The building blocks for the DW parallel to the (110), (120), (130) and (140) planes are shown in Fig. 2(a). Similarly, the reference supercells are constructed and then the supercells with 180° DWs are obtained by applying a twin-like operation on the building blocks of one side, as shown in Fig. 2(b)-(e). Furthermore, the mixed Ising-Bloch-type DWs with anti-parallel Bloch-type components are constructed by displacing the A atoms in the two DWs along +y and -y directions, respectively.

For the 90° DWs, we only consider the head-to-tail polarization configuration for charged neutrality consideration, which is presumably more stable than the head-to-head and tail-to-tail configurations. Because the ferroelastic nature of 90° DWs, the energetically favorable orientation of the DW plane belongs to {110} planes. Fig. 1(c) shows the geometry of the supercell containing the 90° DW, which are oriented to the (101) plane with lattice

parameters $Nc\sqrt{1+(c/a)^2}$, a, and $a\sqrt{1+(c/a)^2}$ in x, y, and z directions, respectively. Here,

N is the number of perovskite unit cells in the supercell with 90° DWs, and a and c are lattice parameters of the unit cell. We notice that the supercells containing 90° DWs of BaTiO₃ were not stable against structural relaxation, which is likely to be ascribed to the fact that tetragonal BTO is not stable phase at 0 K. Therefore, we only consider the 90° DW of PbTiO₃.

Table 1 Description of the supercells constructed (N = 8, 10, 12, 14, 16).

DWs	Degree (°)	Orientation	DW plane	Type	Supercell size	# of atoms	k-point mesh
PTO-A-I	180	(100)	AO	I	$N \times 1 \times 1$	5 <i>N</i>	$1 \times 7 \times 7$
PTO-B-I	180	(100)	BO	I	$N\times1\times1$	5 <i>N</i>	$1\times7\times7$
PTO-A-IB	180	(100)	AO	IB	$16 \times 1 \times 1$	80	$1\times7\times7$
PTO-110-I	180	(110)	ABO	I	$8\sqrt{2}\times\sqrt{2}\times1$	80	$1\times5\times7$
PTO-120-I	180	(120)	AO	I	$4\sqrt{5}\times\sqrt{5}\times1$	100	$1\times4\times7$
PTO-130-I	180	(130)	ABO	I	$4\sqrt{10}\times\sqrt{10}\times1$	200	$1\times3\times7$
PTO-140-I	180	(140)	AO	I	$2\sqrt{17}\times\sqrt{17}\times1$	170	$1\times2\times7$
PTO-110-IB	180	(110)	ABO	IB	$8\sqrt{2}\times\sqrt{2}\times1$	80	$1\times5\times7$
PTO-120-IB	180	(120)	AO	IB	$4\sqrt{5}\times\sqrt{5}\times1$	100	$1\times4\times7$
PTO-130-IB	180	(130)	ABO	IB	$4\sqrt{10}\times\sqrt{10}\times1$	200	$1\times3\times7$
PTO-140 - IB	180	(140)	AO	IB	$2\sqrt{17}\times\sqrt{17}\times1$	170	$1\times2\times7$
PTO-90	90	(101)	ABO	N/A	N/A	5 <i>N</i>	$1\times7\times5$
BTO-A-I	180	(100)	AO	I	$16 \times 1 \times 1$	80	$1\times7\times7$
BTO-B-I	180	(100)	BO	I	$16 \times 1 \times 1$	80	$1\times7\times7$
BTO-110 - I	180	(110)	ABO	I	$8\sqrt{2}\times\sqrt{2}\times1$	80	$1\times5\times7$
BTO-120-I	180	(120)	AO	I	$4\sqrt{5}\times\sqrt{5}\times1$	100	$1\times4\times7$
BTO-130-I	180	(130)	ABO	I	$4\sqrt{10}\times\sqrt{10}\times1$	200	$1\times3\times7$
BTO-140 - I	180	(140)	AO	I	$2\sqrt{17}\times\sqrt{17}\times1$	170	1×2×7

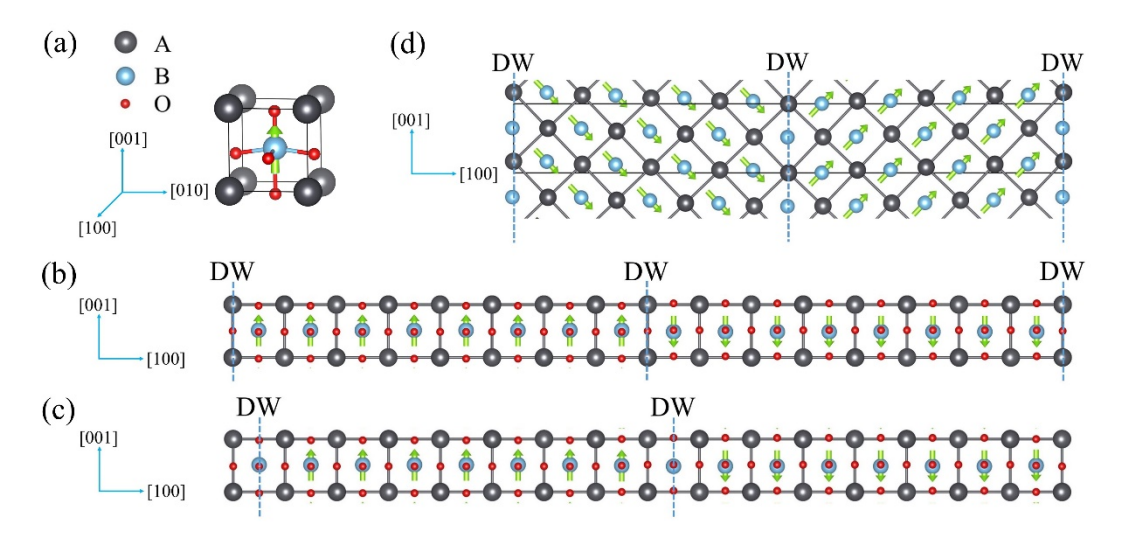


Fig.1. (a) Unit cell of tetragonal ABO₃ perovskite. (b)-(d) Geometry of supercells with (b) A-centered 180° DWs, (c) B-centered 180° DWs and (d) 90° DWs. O atoms in 90° DW structure were not shown.

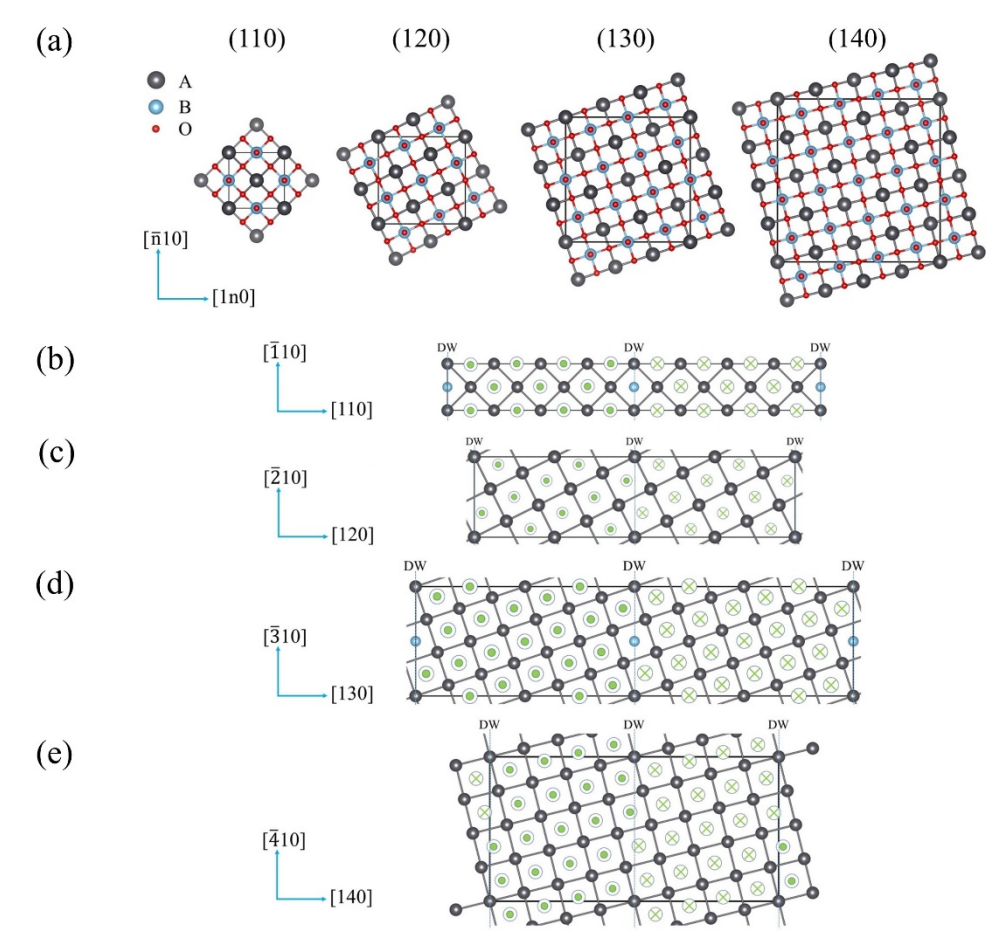


Fig.2. (a) Building blocks of tetragonal ABO₃ perovskite for supercells with (1k0)-oriented 180° DWs construction, (k = 1, 2, 3, 4). Geometry of supercells with (b) (110)-oriented DWs, (c) (120)-oriented DWs, (d) (130)-oriented DWs and (e) (140)-oriented DWs. O atoms in supercells were not shown.

2.3 Three schemes for domain wall energy calculations

In ferroelectric perovskite oxides, the appearance of DWs leads to the change of lattice constants in the proximity of the DWs. The higher the density of DWs, the larger the change of lattice parameters with respect to the single-domain state. The lattice parameters of the supercell with very low density of DWs should approach those of a single domain supercell. The formation energy E_f is expressed as following: $E_f = E_s + 2S\gamma$, where E_s is strain energy, S is the area of DW and γ is DW energy. To accurately evaluate the DW energies, we adopt three structural optimization schemes which can be applied to different situations. We first describe the key steps of each scheme and discuss their applicable conditions. The results of DW energies and structures obtained by using different schemes for the studied materials will be compared and discussed in the next section.

Scheme 1: Fully relaxed supercell with DWs

- (1) Acquire the total energy $E_{\text{bulk},1}$ of the fully relaxed supercell with the DWs by allowing the cell shape, cell volume and atomic positions to relax.
- (2) Construct a supercell with the same supercell size as obtained in Step (1) but without creating the DWs. The two lattice parameters parallel to the DW plane are fixed to be same as those of supercell with DWs; the third lattice parameter and all atomic positions are allowed to relax. The obtained total energy is labeled as $E_{\rm DW,1}$.
- (3) The DW energy $\gamma_1(N)$ in Scheme 1 can be calculated by

$$\gamma_1(N) = \frac{E_{\text{DW},1}(N) - E_{\text{bulk},1}(N)}{2S},$$
 (1)

where S is the area of DW, N is the number of unit cells in the supercell. Then, we calculate $\gamma_1(N)$ for a series of supercells with increasing size N and fit these energies to

$$\gamma_1(N) = k \frac{1}{N} + \gamma_{N \to +\infty}. \tag{2}$$

where k and $\gamma_{N\to +\infty}$ are fitting parameters. The y-intercept of the fitting line, $\gamma_{N\to +\infty}$, is taken as the DW energy in low DW density condition obtained by Scheme 1.

Scheme 2: Fully relaxed bulk supercell

- (1) Acquire the total energy $E_{\text{bulk},2}$ of a fully relaxed bulk supercell, i.e., the $N\times 1\times 1$ reference supercell with uniform polarization configuration.
- (2) Construct a supercell with DWs and fix the lattice parameters to be identical to those of the bulk supercell. Acquire the total energy $E_{DW,2}$ by only relaxing the atomic positions.
- (3) The DW energy $\gamma_2(N)$ in Scheme 2 can be calculated by

$$\gamma_2(N) = \frac{E_{\text{DW},2}(N) - E_{\text{bulk},2}(N)}{2S}.$$
(3)

Note that $\gamma_2(N)$ obtained in this way should show negligible dependence on the domain size and can be taken as the DW energy in the low DW density limit.

Scheme 3: Fully relaxed bulk unit cell

- (1) Acquire the total energy $E_{\text{bulk},3}$ of a fully relaxed bulk unit cell instead of a bulk supercell.
- (2) Construct a supercell containing DWs and fix the lattice parameters the same as those of the bulk unit cell. Acquire the total energy $E_{DW,3}(N)$ by only relaxing the atomic positions.
- (3) The formation energy $E_f(N)$ of a supercell with DWs is calculated by

$$E_{\rm f}(N) = E_{\rm DW,3}(N) - NE_{\rm bulk,3}. \tag{4}$$

We can further write the formation energy in terms of

$$E_{\rm f}(N) = N\xi + 2S\gamma_3,\tag{5}$$

where S represents area of DW, γ_3 is DW energy independent of N, and ζ is a fitting parameter accounting for the energy difference per unit cell between the calculations based on a bulk unit cell and a bulk supercell. We calculate a series of energies $E_f(N)$ with increasing N and fit the data to equation (5). The ζ can be obtained from the slope of the line and the DW energy γ_3 of Scheme 3 can be calculated from the y-intercept divided by 2S.

Scheme 1 can be adopted for the high-density DW (*N* is relatively small) case due to the fully structural optimization of supercell with DWs. While Scheme 2 and Scheme 3 are more applicable for low-density DWs cases, in which the lattice parameters of the supercell with DWs are fixed to be the same as those of a single-domain state. Scheme 3 can be used to calculating all DWs types considered in this work, including some special DW types that cannot be calculated in Scheme 1 and (or) 2. For example, the 90° DW energy of tetragonal phase cannot be calculated in Scheme 1 and 2 because the reference bulk supercell does not satisfy the periodic boundary conditions. In addition, the mixed Ising-Bloch-type 180° DW energies can be calculated in Scheme 2 and 3; in contrast, it leads to an unreasonable negative DW energy when computed using Scheme 1. A comparison of the conditions of applicability and the computational costs between the three schemes is summarized in Table 2.

Table 2 Characteristics and application scenarios of three schemes. "all" in the table 2 represents all DWs structures constructed in this work.

	Scheme 1	Scheme 2	Scheme 3
Experimental situation	high-density (N is small) low-density ($N \rightarrow +\infty$)	low-density	low-density
Applicable DWs structure	except 90° and IB	except 90°	all
Computational cost	small (N is small) large ($N \rightarrow +\infty$)	small	large

2.4 Calculation of spontaneous polarization

The Born effective charge tensor is defined as the proportionality coefficient measuring the polarization change in direction β caused by an atomic displacement in direction α under the conditions of zero external field. The Born effective charge tensor for a given ion i is defined as:

$$Z_{i,\beta\alpha}^* = \frac{\Omega_c}{e} \frac{\partial P_{\beta}}{\partial \mu_{i,\alpha}} \big|_{E=0},\tag{6}$$

where α , β label the Cartesian directions and i labels the atoms. $\mu_{i,\alpha}$ is the coordinate of ion i in the direction α . Ω_c is the volume of the unit cell and e is the electron charge.

The Born effective charge tensor is calculated using the density functional perturbation theory (DFPT)[30] as implemented in VASP. We adopt the "Ti-centered" unit cell proposed in Ref.[11] and choose the center of the eight A atoms as the reference position. The local polarization in the unit cell of j is calculated by

$$\boldsymbol{P}^{(j)} = \frac{e}{a_c} \sum_i w_i \boldsymbol{Z}_i^* (\boldsymbol{\mu}_i^{(j)} - \boldsymbol{u}_0), \tag{7}$$

where $\pmb{\mu}_i^{(j)}$ is the coordinate of atom i in the unit cell j, \pmb{u}_0 is the coordinate of the reference

position, w_i is the weight factor of atom i, and \mathbf{Z}_i^* is the Born effective charge tensor of atom i. The local polarizations are calculated using optimized supercells in Scheme 2.

3 Results and discussion

3.1 Lattice parameters and polarization

The calculated lattice parameters and spontaneous polarization of the unit cell of tetragonal PbTiO₃ and BaTiO₃ are listed in Table 3. The lattice parameters are slightly lower than experimental values of the two pervoskites, which is typical for DFT calculations based on LDA due to the overbinding problem. The largest underestimation of -2.8% is from the lattice parameter c of tetragonal PbTiO₃, which is in accordance with previous calculations[31, 32]. The polarization of bulk tetragonal PbTiO₃ is 74.3 μ C/cm², consistent with experimental measured value of 75 μ C/cm² at room temperature. The polarization is 23.8 μ C/cm² for bulk tetragonal BaTiO₃ which is slightly lower than the experimental values 26 μ C/cm². In general, our calculations give reasonable estimation of the lattice parameters and polarization.

Table 3 Calculated lattice parameters and polarization.

	Twell b emissions invited parameters and perameters.							
		A(Å)	b(Å)	c(Å)	Ref.	$P(\mu C/cm^2)$	Ref.	
	Calc.	3.867	3.867	4.032	this	74.3	this	
PTO	Caic.	3.007	3.007	4.032	work	74.3	work	
	Expt.	3.900	3.900	4.150	[33]	75	[34]	
	Calc.	3.946	3.946	3.992	this	23.8	this	
BTO	Carc.	3.740	3.740	3.772	work	23.0	work	
	Expt.	3.999	3.999	4.022	[35]	26	[36]	

3.2 Domain wall energies of (100)-oriented 180° DWs

The 180° DW energies of tetragonal PbTiO₃ are calculated using the three schemes discussed in Section 2.3.

In Scheme 1, the lattice parameter c becomes smaller and lattice parameter b becomes larger for supercells with DWs compared with those parameters of the unit cell of bulk PbTiO₃. As a result, the c/b ratio becomes smaller in the supercell with DWs, as shown in Fig. 3(b). The c/b ratio approaches the bulk value (1.043) with the increase of supercell size for both Pb-centered and Ti-centered DWs, indicating a decrease of the strain energy in the domains, as shown in Fig. 3(c) and 3(d). In addition, with increasing supercell size, the lattice parameters approach those in bulk and therefore are deviated from those in the DW region, therefore, DW energies increase as shown in Fig. 3(c) and 3(d). As shown in Fig. 3(e) and 3(f), the formation energy density, strain energy density and $2S\gamma_1(N)/N$ decrease with the increase of the size of supercell. Due to the increasing DW energy, the lowering of $2S\gamma_1(N)/N$ arises from the decreasing total area (or density) of DWs.

It is also worth noting that, for the same DW type, the DW energies obtained from Scheme 2 and 3 converge well with each other. For example, the DW energy of Pb-centered Ising-type 180° DW is predicted to be 125.7 mJ/m² and 126.2 mJ/m² using Scheme 2 and 3, respectively. Similarly, for Ti-centered case, the two values of 161.8 mJ/m² and 161.2 mJ/m², respectively. In Schemes 2 and 3, the lattice parameters of supercells with DWs are fixed the same as those of bulk, indicating larger strain (larger c, smaller b and larger c/b) in DW

region, which is consistent with calculated higher DW energies with respect to those calculated in Scheme 1. The fitted result is slightly lower than those obtained in Scheme 2 and 3 for the more stable Pb-centered DWs. In addition, the DW energies are independent of supercell size due to fixed strain (fixed lattice parameters) in DW region as listed in Table 4, indicating the supercell is large enough so that the interaction between the two DWs in the supercell can be ignored. Overall, our results demonstrate the self-consistency between the different schemes in evaluating the DW energies.

As listed in Table 4, the Pb-centered DWs exhibit smaller DW energies for all the schemes, indicating higher stability than the Ti-centered DWs. We fit these energies in Scheme 1 to equation (4) and the fitting results ($N \rightarrow +\infty$) are 118.8 mJ/m² for Pb-centered and 137.3 mJ/m² for Ti-centered DWs, which are lower than DW energies for the low-density case calculated in Scheme 2 and 3.

The Pb-centered and Ti-centered DW energies calculated in Scheme 2 and 3 are about 126 mJ/m² and 162 mJ/m², which are slightly lower than previous theoretical values of 132 mJ/m² for Pb-centered and 169 mJ/m² for Ti-centered DWs calculated by Meyer and Vanderbilt[11] using ultrasoft pseudopotentials (USPP) method with LDA. The calculated 90° DW energy in Scheme 3 is 28.3 mJ/m², which is much lower than the experimental value 50 mJ/m²[37] but agrees well with the theoretical value of 29.2 mJ/m²[38] using the PAW method with LDA and slightly lower than the theoretical value of 35 mJ/m²[11] using the USPP method with LDA.

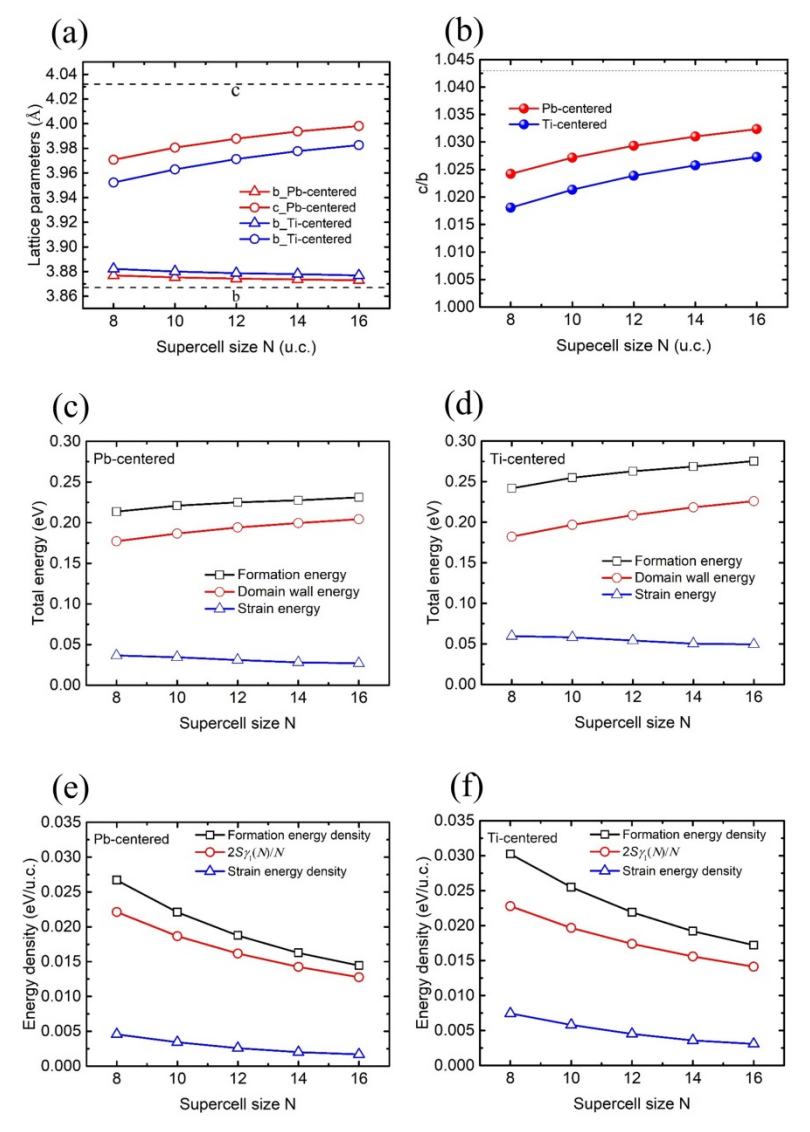


Fig.3. The calculated (a) lattice parameters and (b) c/b ratio of supercells as a function of the supercell size N for Pb- and Ti-centered DWs optimized in Scheme 1. The dash lines in (a) and (b) are calculated lattice parameters b, c and c/b in bulk, respectively. Total energy of supercells as a function of the supercell size N for (c) Pb-centered and (d) Ti-centered DWs. Energy density of supercells as a function of the supercell size N for (e) Pb-centered and (f) Ti-centered DWs.

Similar to PbTiO₃, the same energy sequence for both DW plane types and structural optimization schemes hold for tetragonal BaTiO₃, but with much lower DW energies, as listed in Table 5. In Scheme 2, the calculated Ba-centered and Ti-centered 180° DW of tetragonal BaTiO₃ are 6.0 mJ/m² and 13.9 mJ/m², which are slightly lower than the values of 7.5 mJ/m² for Ba-centered and 16.8 mJ/m² for Ti-centered DWs in Ref.[11] and much lower than 14.8 mJ/m² and 85.5 mJ/m² in Ref.[12]. The disagreements between our calculations and work in Ref.[12] may be due to different calculation schemes and choice of pseudopotentials.

For PbTiO₃, the mixed Ising-Bloch-type DWs exhibit lower DW energies than Ising-type for A-centered type, as listed in Table 5. For the mixed Ising-Bloch-type DWs of the B-centered type, our calculations lead to an unstable structure during the structural optimization. Therefore, we did not include the results here.

	Schei	me 1	Sche	eme 2		Scheme 3	
N -	180°	180°	180°	180°	180°	180°	90°
1 v -	Pb-	Ti-	Pb-	Ti-	Pb-	Ti-	Pb-Ti-O
	centered						
8	92.1	95.2	125.9	161.8	_	_	_
10	96.9	102.5	125.7	161.5	_		_
12	100.6	108.5	125.5	161.3	_	_	_
14	103.3	113.4	125.8	162.1	_		_
16	105.7	116.2	125.7	162.4	_		_
Fitted results	118.8	137.3	_	_	126.2	161.2	28.3

Table 5 Calculated (100)-oriented Ising-type and Ising-Bloch-type 180° domain wall energies (mJ/m²) using supercells with 16 unit cells.

	Sche	me 1	Sche	me 2
	A-centered	B-centered	A-centered	B-centered
PTO-A(B)-I	105.7	116.2	125.7	162.4
BTO-A(B)-I	5.8	11.2	6.0	13.9
PTO-A-IB			120.2	_

3.3 Anisotropy of domain wall energies

The calculated DW energies of A-centered 180° DWs of the tetragonal phase with different orientations are shown in Fig. 4. The (110)-oriented 180° DWs exhibit the largest DW energies for both PbTiO₃ and BaTiO₃, indicating (110) is the most unfavorable orientation, consistent with investigation on PbTiO₃ by Pökkö et al[18]. In addition, the (130)-oriented 180° DWs also exhibit high DW energies. The B atoms are in the center of the DW plane for both (110)-oriented and (130)-oriented DWs, which is consistent with the calculations that B-centered (100)-oriented DWs exhibit higher DW energies than those of A-centered (100)-oriented DWs. For BaTiO₃, (140)-oriented DW energy is close to that of (100)-oriented DW, which agrees with previous calculations[12].

The DW energy anisotropic factor for orientation i can be defined as $K_i = \frac{\sqrt{(\gamma_i - \bar{\gamma})^2}}{\bar{\gamma}}$, where $\bar{\gamma}$ is the average value of DW energies of different orientations, which is defined as isotropic parts. The $\sqrt{(\gamma_i - \bar{\gamma})^2}$ is defined as anisotropic parts. Larger $\sum K_i$ values indicate larger anisotropy. The $K_{(110)}$ is the largest for both PbTiO₃ and BaTiO₃, taking more than 42% of sum of all the anisotropic factors. As listed in Table 6, the BaTiO₃ generally exhibits larger anisotropy than PbTiO₃ in terms of the 180° DW energies with larger anisotropic factors, which is consistent with the study by Hlinka et al.[39]. Note that Ref [37] estimates the anisotropy of the two materials by analyzing the experimental phonon spectra. Here, our results provide evidence from first-principles calculations verifying the experimental findings.

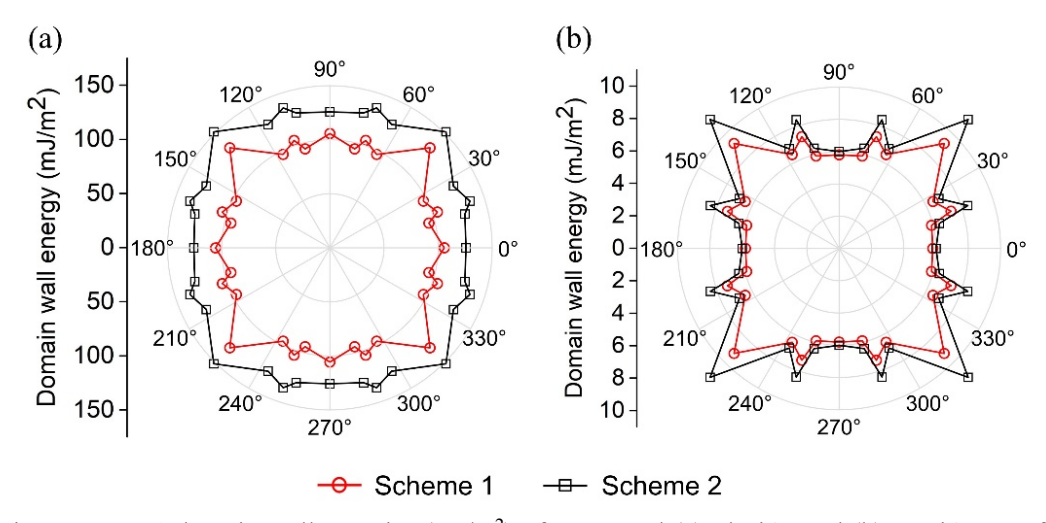


Fig.4. Ising-type 180° domain wall energies (mJ/m²) of tetragonal (a) PbTiO₃ and (b) BaTiO₃ as a function of the rotation angle of the domain wall plane around [001]. The angle 0° corresponds to the normal of the DW plane along [100] and 90° corresponds to the normal of domain wall plane along [010].

Table 6 Calculated anisotropic factors of orientation dependent Ising-type and mixed Ising-Bloch-type 180° DWs.

	Scheme	$K_{(100)}$	$K_{(110)}$	$K_{(120)}$	$K_{(130)}$	$K_{(140)}$	$\sum_i K_i$
PTO-I	1	0.0068	0.2291	0.0923	0.0162	0.1139	0.4582
PTO-I	2	0.0619	0.1321	0.0478	0.0179	0.0403	0.3000
BTO-I	1	0.1643	0.3256	0.0634	0.0519	0.1499	0.7550
BTO-I	2	0.2308	0.4487	0.1154	0.0769	0.1795	1.0513
PTO-IB	2	0.0535	0.0947	0.0189	0.0110	0.0102	0.1874

Compared with pure Ising-type 180° DWs, the mixed Ising-Bloch-type 180° DWs exhibit slightly lower DW energies for all orientations for tetragonal PbTiO₃ as shown in Fig. 5. This finding suggests that the emergence of the Bloch-type component increases the stability of 180° DWs of tetragonal PbTiO₃ regardless of the DW orientations. Moreover, the existence of the Bloch-type component also changes the anisotropy of the DW energies, as shown in Fig. 5 and their anisotropic factors in Table 6. Compared with pure Ising-type DWs, the Ising-Bloch-type DWs of tetragonal PbTiO₃ becomes more isotropic with respect to different orientations.

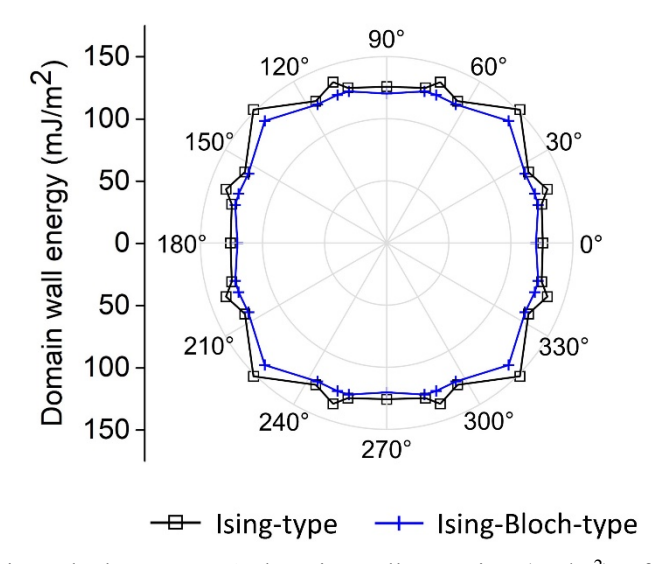


Fig.5. Ising-type and Ising-Bloch-type 180° domain wall energies (mJ/m²) of tetragonal PbTiO₃ as a function of the rotation angle in Scheme 2.

3.4 Polarization profiles across the domain walls

We further examine the distribution of the ferroelectric polarization across the 180° DWs with different orientations. The polarization profiles of (1k0)-oriented (k = 1, 2, 3, 4) Isingtype and mixed Ising-Bloch-type 180° DWs of tetragonal PbTiO₃ optimized in Scheme 2 are shown in Fig. 6. For the Ising-type 180° DWs of PbTiO₃, the polarization in the region far away from DW is close to that in bulk. The polarization reduces abruptly to zero in the center of DW and reincreases to its bulk value in the opposite direction. The width of 180° DW is measured to be less than 10 Å, showing excellent agreement with atomic-force microscopy observation[40]. On the other hand, stable Bloch components can be obtained regardless of orientations. For Ising-Bloch-type 180° DW of PbTiO₃, the Bloch-type component P_{y} in the (100)-oriented DWs peaks at the DW center to be 25.5 μC/cm², which is more than one third of the Ising component P_z . Our calculation is much lower than the maximum Bloch-type component 65 μ C/cm² in Ref. [41], but consistent with the value of 28.4 μ C/cm² obtained by the first-principles calculation in Ref. [17]. Among all (1k0)-oriented DWs we studied, the (110)-oriented DW manifests a maximal Bloch-type component with the value of 34.7 μC/cm². Meanwhile, it also shows the largest difference in the DW energy relative to the corresponding Ising-type DW. If we define the width at half height of the peak of Bloch-type component polarization profile to be the width of the mixed Ising-Bloch-type DWs, the width of the mixed Ising-Bloch-type DW of PbTiO₃ is around 7.4 Å, almost independent of the DWs orientation and supercell size. In addition, the Ising component P_z of the mixed Ising-Bloch-type DWs does not deviate much from that of the Ising-type DWs, indicating the P_z and P_{ν} components are weakly coupled in the IB-type DWs.

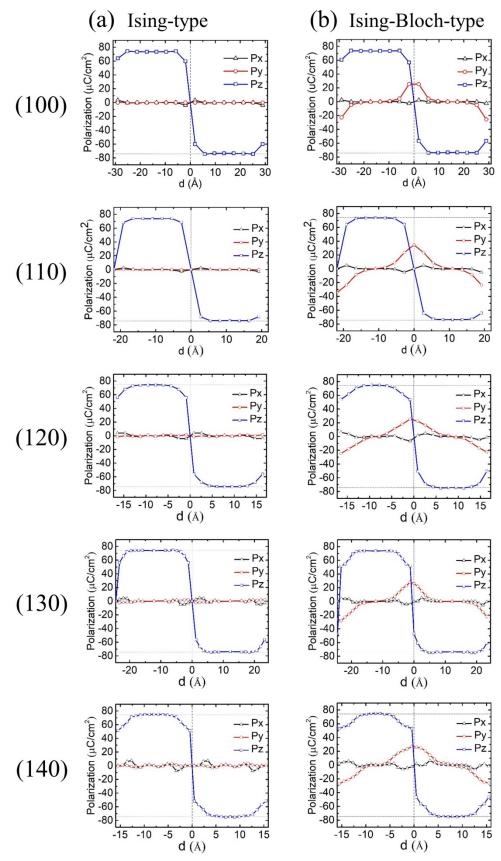


Fig.6. The polarization profiles of (1k0)-oriented DWs (k = 0, 1, 2, 3, 4) of PbTiO₃. (a) Ising-type, (b) Ising-Bloch-type. The horizontal dash lines indicate the magnitude of polarization in the bulk. Herein d is the distance away from the central domain wall plane.

4 Summary

In this study, we have adopted three structural optimization schemes to calculate the energies of various types of 180° and 90° DWs for two prototypical tetragonal ferroelectric perovskites, PbTiO₃ and BaTiO₃. Many subtleties that affect the values of DW energies have been carefully examined, including the centered atom in the DW plane, system size, DW orientation, presence of non-Ising polarization components. In particular, we evaluated the anisotropy of 180° DW energies for Ising-type DWs of PbTiO₃ and BaTiO₃ and Ising-Blochtype DWs of PbTiO₃. The results showed that

- (1) The value of DW energies can be influenced by the different schemes for structural relaxation of the supercells. This dependence can explain the scattered values of DW energies and the discrepancy in the prediction of non-Ising type DWs reported in previous studies using first-principles calculations. We also demonstrated that a self-consistent result on the DW energies can be achieved by using the proposed structural relaxation Scheme 2 and 3.
- (2) The anisotropy of 180° DW energy is larger in tetragonal BaTiO₃ than that in tetragonal PbTiO₃. For both materials, the (110)-oriented 180° DW exhibit the highest DW energies. Our *ab initio* results verified the previous estimation on the DW anisotropy for the two materials based on experimental measurements and LGD theory[37].
- (3) The presence of Bloch-type component in the mixed Ising-Bloch-type DWs lowers the DW energies of tetragonal PbTiO₃, leading to more isotropic DW energies. The knowledge on the stability of non-Ising type DWs can be useful to guide the domain wall engineering for advanced ferroelectrics-based nanoelectronics[42].

Acknowledgements

X. Y. Z. acknowledges the support from Tsinghua Scholarship for Overseas Graduate Studies (No. 2018088) and Major Program of National Natural Science Foundation of China (No. 51790494). B.W. acknowledges support by the National Science Foundation (NSF) through Grant No. DMR-1744213. Y. W. and L. Q. C. acknowledge the generous support by the Hamer Foundation through a Hamer Professorship at Penn State. This work partially used the Extreme Science and Engineering Discovery Environment (XSEDE), which is supported by National Science Foundation grant number ACI-1548562. The authors thank Ben Xu for the support of computational resources.

References

- [1] C. Stefani, L. Ponet, K. Shapovalov, P. Chen, E. Langenberg, D.G. Schlom, S. Artyukhin, M. Stengel, N. Domingo, G. Catalan, Mechanical Softness of Ferroelectric 180° Domain Walls, Physical Review X 10(4) (2020) 041001.
- [2] D. Ghosh, A. Sakata, J. Carter, P.A. Thomas, H. Han, J.C. Nino, J.L. Jones, Domain Wall Displacement is the Origin of Superior Permittivity and Piezoelectricity in BaTiO₃ at Intermediate Grain Sizes, Advanced Functional Materials 24(7) (2014) 885-896.
- [3] N. Bassiri-Gharb, I. Fujii, E. Hong, S. Trolier-McKinstry, D.V. Taylor, D. Damjanovic, Domain wall

- contributions to the properties of piezoelectric thin films, Journal of Electroceramics 19(1) (2007) 49-67.
- [4] J. Seidel, L.W. Martin, Q. He, Q. Zhan, Y.H. Chu, A. Rother, M.E. Hawkridge, P. Maksymovych, P. Yu, M. Gajek, N. Balke, S.V. Kalinin, S. Gemming, F. Wang, G. Catalan, J.F. Scott, N.A. Spaldin, J. Orenstein, R. Ramesh, Conduction at domain walls in oxide multiferroics, Nat Mater 8(3) (2009) 229-34.
- [5] J. Ma, J. Ma, Q. Zhang, R. Peng, J. Wang, C. Liu, M. Wang, N. Li, M. Chen, X. Cheng, P. Gao, L. Gu, L.Q. Chen, P. Yu, J. Zhang, C.W. Nan, Controllable conductive readout in self-assembled, topologically confined ferroelectric domain walls, Nat Nanotechnol 13(10) (2018) 947-952.
- [6] M.-M. Yang, A. Bhatnagar, Z.-D. Luo, M. Alexe, Enhancement of Local Photovoltaic Current at Ferroelectric Domain Walls in BiFeO₃, Scientific Reports 7(1) (2017) 43070.
- [7] A. Bhatnagar, A. Roy Chaudhuri, Y. Heon Kim, D. Hesse, M. Alexe, Role of domain walls in the abnormal photovoltaic effect in BiFeO₃, Nature Communications 4(1) (2013) 2835.
- [8] Y.A. Genenko, J. Glaum, M.J. Hoffmann, K. Albe, Mechanisms of aging and fatigue in ferroelectrics, Materials Science and Engineering: B 192 (2015) 52-82.
- [9] W. Cao, L.E. Cross, Theory of tetragonal twin structures in ferroelectric perovskites with a first-order phase transition, Physical Review B 44(1) (1991) 5-12.
- [10] J. Hlinka, P. Márton, Phenomenological model of a 90° domain wall in BaTiO₃-type ferroelectrics, Physical Review B 74(10) (2006) 104104.
- [11] B. Meyer, D. Vanderbilt, Ab initio study of ferroelectric domain walls in PbTiO₃, Physical Review B 65(10) (2002) 104111.
- [12] M. Li, Y. Gu, Y. Wang, L.-Q. Chen, W. Duan, First-principles study of 180° domain walls in BaTiO₃: Mixed Bloch-Néel-Ising character, Physical Review B 90(5) (2014) 054106.
- [13] Y. Wang, C. Nelson, A. Melville, B. Winchester, S. Shang, Z.-K. Liu, D.G. Schlom, X. Pan, L.-Q. Chen, BiFeO₃ Domain Wall Energies and Structures: A Combined Experimental and Density Functional Theory+U Study, Physical Review Letters 110(26) (2013) 267601.
- [14] O. Diéguez, P. Aguado-Puente, J. Junquera, J. Íñiguez, Domain walls in a perovskite oxide with two primary structural order parameters: First-principles study of BiFeO₃, Physical Review B 87(2) (2013) 024102.
- [15] R.K. Behera, C.-W. Lee, D. Lee, A.N. Morozovska, S.B. Sinnott, A. Asthagiri, V. Gopalan, S.R. Phillpot, Structure and energetics of 180° domain walls in PbTiO₃ by density functional theory, Journal of Physics: Condensed Matter 23(17) (2011) 175902.
- [16] D. Lee, R.K. Behera, P. Wu, H. Xu, Y.L. Li, S.B. Sinnott, S.R. Phillpot, L.Q. Chen, V. Gopalan, Mixed Bloch-Néel-Ising character of 180° ferroelectric domain walls, Physical Review B 80(6) (2009) 060102.
- [17] Y.J. Wang, D. Chen, Y.L. Tang, Y.L. Zhu, X.L. Ma, Origin of the Bloch-type polarization components at the 180° domain walls in ferroelectric PbTiO₃, Journal of Applied Physics 116(22) (2014) 224105.
- [18] S. Pöykkö, D.J. Chadi, Ab initio study of 180° domain wall energy and structure in PbTiO₃, Applied Physics Letters 75(18) (1999) 2830-2832.
- [19] S. Pöykkö, D.J. Chadi, Ab initio study of dipolar defects and 180° domain walls in PbTiO₃, Journal of Physics and Chemistry of Solids 61(2) (2000) 291-294.
- [20] J. Padilla, W. Zhong, D. Vanderbilt, First-principles investigation of 180° domain walls in BaTiO₃, Physical Review B 53(10) (1996) R5969-R5973.
- [21] Y. Gu, M. Li, A.N. Morozovska, Y. Wang, E.A. Eliseev, V. Gopalan, L.-Q. Chen, Flexoelectricity and ferroelectric domain wall structures: Phase-field modeling and DFT calculations, Physical Review B 89(17) (2014) 174111.
- [22] P.V. Yudin, A.K. Tagantsev, E.A. Eliseev, A.N. Morozovska, N. Setter, Bichiral structure of ferroelectric domain walls driven by flexoelectricity, Physical Review B 86(13) (2012).

- [23] M.A.E.-S. Pereira Gonçalves, C.; Garca-Fernández, P.; Junquera, J.; Íñiguez, J., Theoretical Guidelines to Create and Tune Electric Skyrmion Bubbles, Science Advances 5(2) (2019) eaau7023.
- [24] D. Lee, H. Xu, V. Dierolf, V. Gopalan, S.R. Phillpot, Structure and energetics of ferroelectric domain walls in LiNbO₃ from atomic-level simulations, Physical Review B 82(1) (2010) 014104.
- [25] P.E. Blöchl, Projector augmented-wave method, Physical Review B 50(24) (1994) 17953-17979.
- [26] G. Kresse, J. Furthmüller, Efficiency of ab-initio total energy calculations for metals and semiconductors using a plane-wave basis set, Computational Materials Science 6(1) (1996) 15-50.
- [27] G. Kresse, D. Joubert, From ultrasoft pseudopotentials to the projector augmented-wave method, Physical Review B 59(3) (1999) 1758-1775.
- [28] D.M. Ceperley, B.J. Alder, Ground State of the Electron Gas by a Stochastic Method, Physical Review Letters 45(7) (1980) 566-569.
- [29] K. Momma, F. Izumi, VESTA 3 for three-dimensional visualization of crystal, volumetric and morphology data, Journal of Applied Crystallography 44(6) (2011) 1272-1276.
- [30] M. Gajdoš, K. Hummer, G. Kresse, J. Furthmüller, F. Bechstedt, Linear optical properties in the projector-augmented wave methodology, Physical Review B 73(4) (2006) 045112.
- [31] X. Wang, T. Xu, F. Xuan, C. Chen, T. Shimada, T. Kitamura, Effect of the oxygen vacancy on the ferroelectricity of 90° domain wall structure in PbTiO₃: A density functional theory study, Journal of Applied Physics 126(17) (2019) 174107.
- [32] Y. Zhang, J. Sun, J.P. Perdew, X. Wu, Comparative first-principles studies of prototypical ferroelectric materials by LDA, GGA, and SCAN meta-GGA, Physical Review B 96(3) (2017) 035143.
- [33] J. Suchanicz, K. Wojcik, Effect of external stress on dielectric properties of PbTiO₃ single crystal, Materials Science and Engineering: B 104(1) (2003) 31-35.
- [34] M.J. Haun, E. Furman, S.J. Jang, H.A. McKinstry, L.E. Cross, Thermodynamic theory of PbTiO₃, Journal of Applied Physics 62(8) (1987) 3331-3338.
- [35] C.J. Xiao, C.Q. Jin, X.H. Wang, Crystal structure of dense nanocrystalline BaTiO₃ ceramics, Materials Chemistry and Physics 111(2) (2008) 209-212.
- [36] H.H. Wieder, Electrical Behavior of Barium Titanatge Single Crystals at Low Temperatures, Physical Review 99(4) (1955) 1161-1165.
- [37] S. Stemmer, S.K. Streiffer, F. Ernst, M. Rüuhle, Atomistic structure of 90° domain walls in ferroelectric PbTiO₃ thin films, Philosophical Magazine A 71(3) (1995) 713-724.
- [38] T. Shimada, Y. Umeno, T. Kitamura, Ab initio study of stress-induced domain switching in PbTiO₃, Physical Review B 77(9) (2008) 094105.
- [39] J. Hlinka, Domain Walls of BaTiO3and PbTiO3Within Ginzburg-Landau-Devonshire Model, Ferroelectrics 375(1) (2008) 132-137.
- [40] Y.G. Wang, J. Dec, W. Kleemann, Study on surface and domain structures of PbTiO₃ crystals by atomic force microscopy, Journal of Applied Physics 84(12) (1998) 6795-6799.
- [41] J.C. Wojdel, J. Iniguez, Ferroelectric transitions at ferroelectric domain walls found from first principles, Phys Rev Lett 112(24) (2014) 247603.
- [42] D. Meier, S.M. Selbach, Ferroelectric domain walls for nanotechnology, Nature Reviews Materials 7(3) (2022) 157-173.

Figure Captions:

- Fig.1. (a) Unit cell of tetragonal ABO₃ perovskite. (b)-(d) Geometry of supercells with (b) A-centered 180° DWs, (c) B-centered 180° DWs and (d) 90° DWs. O atoms in 90° DW structure were not shown.
- Fig.2. (a) Building blocks of tetragonal ABO₃ perovskite for supercells with (1k0)-oriented 180° DWs construction, (k = 1, 2, 3, 4). Geometry of supercells with (b) (110)-oriented DWs, (c) (120)-oriented DWs, (d) (130)-oriented DWs and (e) (140)-oriented DWs. O atoms in supercells were not shown.
- Fig.3. The calculated (a) lattice parameters and (b) c/b ratio of supercells as a function of the supercell size N for Pb- and Ti-centered DWs optimized in Scheme 1. The dash lines in (a) and (b) are calculated lattice parameters b, c and c/b in bulk, respectively. Total energy of supercells as a function of the supercell size N for (c) Pb-centered and (d) Ti-centered DWs. Energy density of supercells as a function of the supercell siIN for (e) Pb-centered and (f) Ti-centered DWs.
- Fig.4. Ising-type 180° domain wall energies (mJ/m²) of tetragonal (a) PbTiO₃ and (b) BaTiO₃ as a function of the rotation angle of the domain wall plane around [001]. The angle 0° corresponds to the normal of the DW plane along [100] and 90° corresponds to the normal of domain wall plane along [010].
- Fig.5. Ising-type and Ising-Bloch-type 180° domain wall energies (mJ/m²) of tetragonal PbTiO₃ as a function of the rotation angle in Scheme 2.
- Fig.6. The polarization profiles of (1k0)-oriented DWs (k = 0, 1, 2, 3, 4) of PbTiO₃. (a) Ising-type, (b) Ising-Bloch-type. The horizontal dash lines indicate the magnitude of polarization in the bulk. Herein d is the distance away from the central domain wall plane.

Table Captions:

Table 1 Description of the supercells constructed (N = 8, 10, 12, 14, 16)

Table 2 Characteristics and application scenarios of three schemes. All represent all DWs structures constructed in this work.

Table 3 Calculated lattice parameters and polarization.

Table 4 Calculated 90° and Ising-type 180° domain wall energies (mJ/m²) of tetragonal PbTiO₃.

Table 5 Calculated (100)-oriented Ising-type and Ising-Bloch-type 180° domain wall energies (mJ/m²) using supercells with 16 unit cells.

Table 6 Calculated anisotropic factors of orientation dependent Ising-type and mixed Ising-Bloch-type 180° DWs.

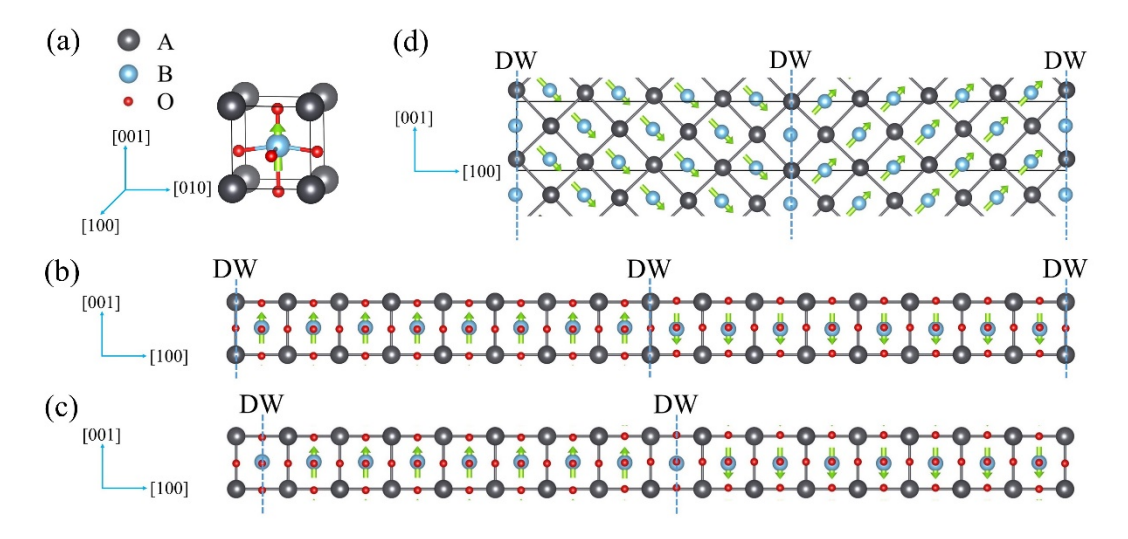


Fig.1. (a) Unit cell of tetragonal ABO₃ perovskite. (b)-(d) Geometry of supercells with (b) A-centered 180° DWs, (c) B-centered 180° DWs and (d) 90° DWs. O atoms in 90° DW structure were not shown.

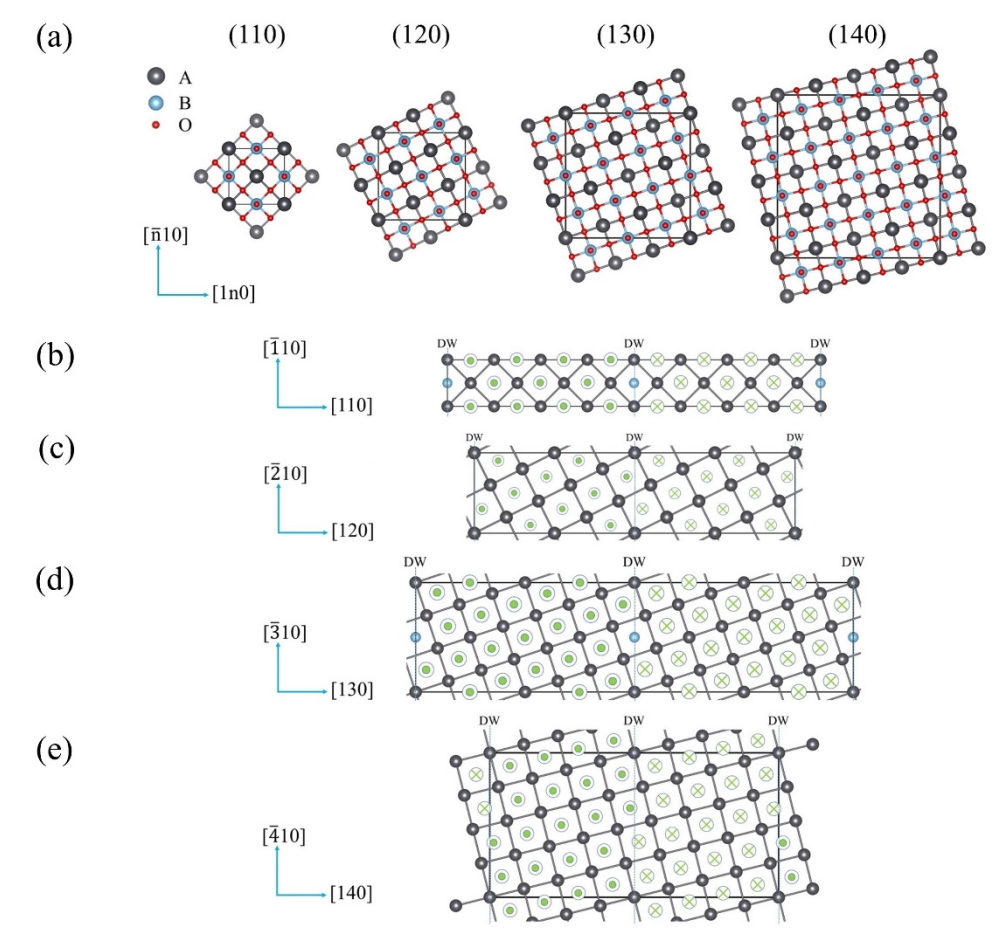


Fig.2. (a) Building blocks of tetragonal ABO₃ perovskite for supercells with (1k0)-oriented 180° DWs construction, (k = 1, 2, 3, 4). Geometry of supercells with (b) (110)-oriented DWs, (c) (120)-oriented DWs, (d) (130)-oriented DWs and (e) (140)-oriented DWs. O atoms in supercells were not shown.

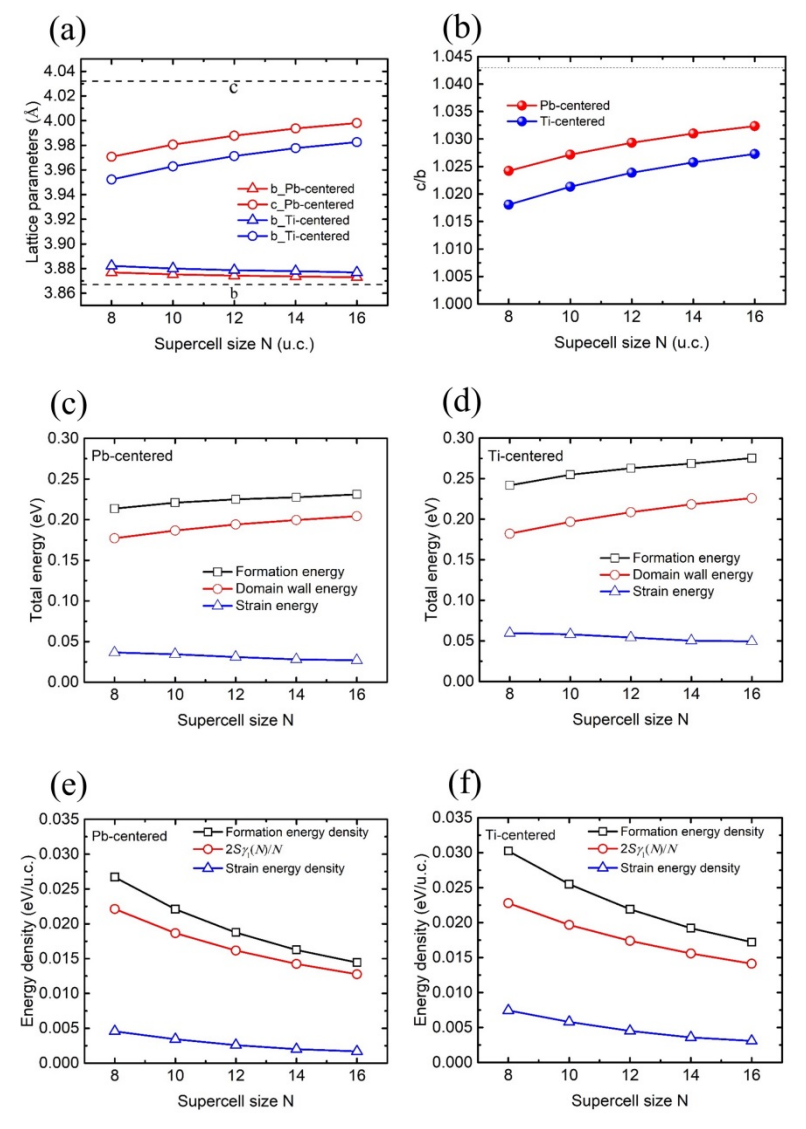


Fig.3. The calculated (a) lattice parameters and (b) c/b ratio of supercells as a function of the supercell size N for Pb- and Ti-centered DWs optimized in Scheme 1. The dash lines in (a) and (b) are calculated lattice parameters b, c and c/b in bulk, respectively. Total energy of supercells as a function of the supercell size N for (c) Pb-centered and (d) Ti-centered DWs. Energy density of supercells as a function of the supercell size N for (e) Pb-centered and (f) Ti-centered DWs.

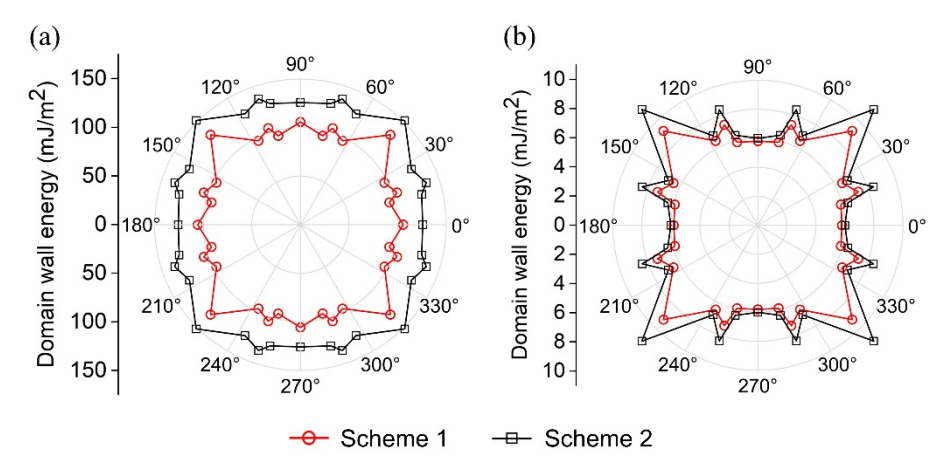


Fig.4. Ising-type 180° domain wall energies (mJ/m²) of tetragonal (a) PbTiO₃ and (b) BaTiO₃ as a function of the rotation angle of the domain wall plane around [001]. The angle 0° corresponds to the normal of the DW plane along [100] and 90° corresponds to the normal of domain wall plane along [010].

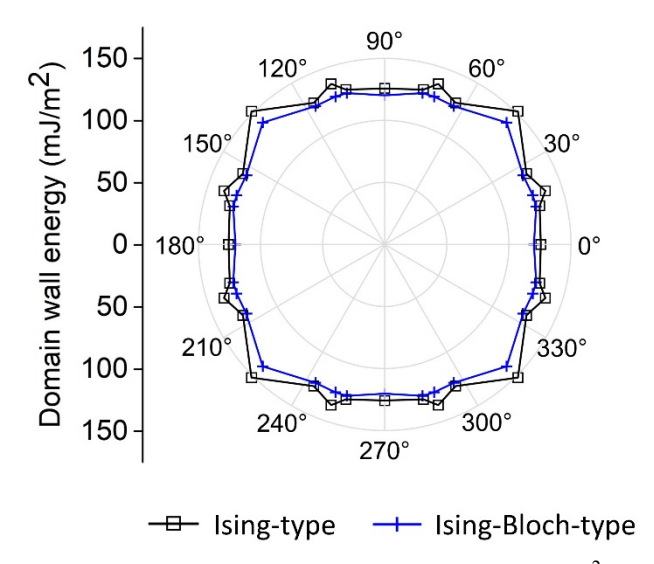


Fig.5. Ising-type and Ising-Bloch-type 180° domain wall energies (mJ/m²) of tetragonal PbTiO₃ as a function of the rotation angle in Scheme 2.

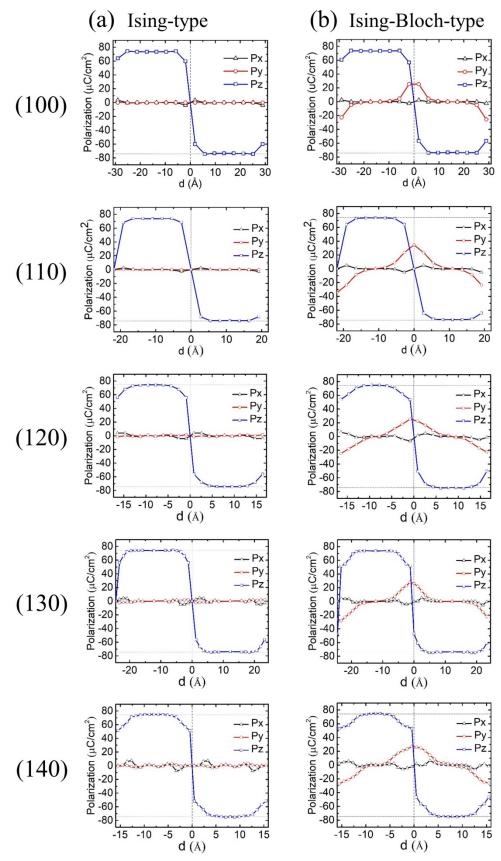


Fig.6. The polarization profiles of (1k0)-oriented DWs (k = 0, 1, 2, 3, 4) of PbTiO₃. (a) Ising-type, (b) Ising-Bloch-type. The horizontal dash lines indicate the magnitude of polarization in the bulk. Herein d is the distance away from the central domain wall plane.

Table 1 Description of the supercells constructed (N = 8, 10, 12, 14, 16).

DWs	Degree	Orien	DW	Tyma	Supercell size	# of	k -point
DWS	(°)	tation	plane	Type	Supercen size	atoms	mesh
PTO-A-I	180	(100)	AO	I	$N\times1\times1$	5 <i>N</i>	$1\times7\times7$
PTO-B-I	180	(100)	ВО	I	$N\times1\times1$	5 <i>N</i>	$1\times7\times7$
PTO-A-IB	180	(100)	AO	IB	$16 \times 1 \times 1$	80	$1\times7\times7$
PTO-110-I	180	(110)	ABO	I	$8\sqrt{2}\times\sqrt{2}\times1$	80	$1\times5\times7$
PTO-120-I	180	(120)	AO	I	$4\sqrt{5}\times\sqrt{5}\times1$	100	$1\times4\times7$
PTO-130-I	180	(130)	ABO	I	$4\sqrt{10}\times\sqrt{10}\times1$	200	$1\times3\times7$
PTO-140-I	180	(140)	AO	I	$2\sqrt{17}\times\sqrt{17}\times1$	170	$1\times2\times7$
PTO-110-IB	180	(110)	ABO	IB	$8\sqrt{2}\times\sqrt{2}\times1$	80	$1\times5\times7$
PTO-120-IB	180	(120)	AO	IB	$4\sqrt{5}\times\sqrt{5}\times1$	100	$1\times4\times7$
PTO-130-IB	180	(130)	ABO	IB	$4\sqrt{10}\times\sqrt{10}\times1$	200	$1\times3\times7$
PTO-140-IB	180	(140)	AO	IB	$2\sqrt{17}\times\sqrt{17}\times1$	170	$1\times2\times7$
PTO-90	90	(101)	ABO	N/A	N/A	5 <i>N</i>	$1\times7\times5$
BTO-A-I	180	(100)	AO	I	$16 \times 1 \times 1$	80	$1\times7\times7$
BTO-B-I	180	(100)	ВО	I	$16 \times 1 \times 1$	80	$1\times7\times7$
BTO-110 - I	180	(110)	ABO	I	$8\sqrt{2}\times\sqrt{2}\times1$	80	$1\times5\times7$
BTO-120 - I	180	(120)	AO	I	$4\sqrt{5}\times\sqrt{5}\times1$	100	$1\times4\times7$
BTO-130-I	180	(130)	ABO	I	$4\sqrt{10}\times\sqrt{10}\times1$	200	$1\times3\times7$
BTO-140-I	180	(140)	AO	I	$2\sqrt{17}\times\sqrt{17}\times1$	170	1×2×7

Table 2 Characteristics and application scenarios of three schemes. All represent all DWs structures constructed in this work.

	Scheme 1	Scheme 2	Scheme 3
Experimental situation	high-density (N is small) low-density ($N \rightarrow +\infty$)	low-density	low-density
Applicable DWs structure	except 90° and IB	except 90°	all
Computational cost	small (N is small) large ($N \rightarrow +\infty$)	small	large

Table 3 Calculated lattice parameters and polarization.

		a(Å)	b(Å)	c(Å)	Ref.	$P(\mu C/cm^2)$	Ref.
РТО	Calc.	3.867	3.867	4.032	this work	74.3	this work
	Expt.	3.900	3.900	4.150	[33]	75	[34]
ВТО	Calc.	3.946	3.946	3.992	this work	23.8	this work
	Expt.	3.999	3.999	4.022	[35]	26	[36]

Table 4 Calculated 90° and Ising-type 180° domain wall energies (mJ/m²) of tetragonal PbTiO₃.

	Schen	ne 1	Sche	eme 2		Scheme 3	
<i>N</i> -	180°	180°	180°	180°	180°	180°	90°
1 V =	Pb-	Ti-	Pb-	Ti-	Pb-	Ti-	Pb-Ti-O
	centered						
8	92.1	95.2	125.9	161.8			_
10	96.9	102.5	125.7	161.5			_
12	100.6	108.5	125.5	161.3			_
14	103.3	113.4	125.8	162.1			_
16	105.7	116.2	125.7	162.4			_
Fitting results	118.8	137.3	_	_	126.2	161.2	28.3

Table 5 Calculated (100)-oriented Ising-type and Ising-Bloch-type 180° domain wall energies (mJ/m²) using supercells with 16 unit cells.

	Sche	me 1	Sche	me 2
	A-centered	B-centered	A-centered	B-centered
PTO-A(B)-I	105.7	116.2	125.7	162.4
BTO-A(B)-I	5.8	11.2	6.0	13.9
PTO-A(B)-IB	_	_	120.2	_

Table 6 Calculated anisotropic factors of orientation dependent Ising-type and mixed Ising-Bloch-type 180° DWs.

	Scheme	$K_{(100)}$	K ₍₁₁₀₎	K ₍₁₂₀₎	$K_{(130)}$	$K_{(140)}$	$\sum_i K_i$
PTO-I	1	0.0068	0.2291	0.0923	0.0162	0.1139	0.4582
PTO-I	2	0.0619	0.1321	0.0478	0.0179	0.0403	0.3000
BTO-I	1	0.1643	0.3256	0.0634	0.0519	0.1499	0.7550
BTO-I	2	0.2308	0.4487	0.1154	0.0769	0.1795	1.0513
PTO-IB	2	0.0535	0.0947	0.0189	0.0110	0.0102	0.1874